As can be seen in Table 2, the agreement between the trace metal residence times based on stream flow and sedimentation rate is, with the exception of those for Cd, quite good and certainly better than other recent comparisons[10,14]. Furthermore, the calculated influx of fluvial suspended particulate matter is comparable with the rate of oceanic sedimentation[13]. The discrepancy between the calculated rate of cadmium input to the oceans by rivers and the rate of cadmium sedimentation is too large to be attributed solely to an abnormality in the composition of the St Lawrence River, especially in view of a recent analysis of Amazon River water[11]. It is probable that the sedimentation rate is a more realistic estimate of oceanic throughput than river input in this case but some re-examination of both the extent of nearshore precipitation and the Cd distribution in marine sediments seems warranted. Co and Ni are the only elements for which the stream flow residence times are greater than the sedimentation rate residence times. This suggests that other forms of input are more important for these elements than the others. It is interesting that when the relative metal contents of terrigenous rock and corrected river flux are compared, Co and Ni are the only elements which are enriched in terrigenous rock. Dry atmospheric fallout may, therefore, be more important for Co and Ni than for the other elements.

Overall, our estimates of residence time are generally shorter than values given in previous compilations[15,16]. This feature is most pronounced in the cases of Fe and Mn. Labeyrie *et al.*[17] have estimated, on the basis of weapon-produced $^{55}Fe$ settling rates, that the residence time of Fe is about 10 yr. We are thus not alone in proposing such a short residence time for this element. Concern has often been expressed about the difficulty of rationalising residence times much shorter than oceanic mixing times with evidence for the relatively homogeneous distribution of the same elements in ocean sediments. This conflict will be reconciled if biological activity and horizontal dispersion/mixing of both particulate and dissolved metals is sufficient to ensure reasonably uniform metal concentrations in surface waters beyond the continental shelves. Settling of the inorganic and refractory biogenic components of the uniformly distributed particulate matter will then account for the relatively uniform distribution of the metals in the sediments. The residence time of Fe in the surface layer of the open ocean, calculated according to the method of Goldberg *et al.*[16] and using data from the western North Atlantic[9], is 16 yr compared with 20 yr for water. Mn, unlike most other metals, has a concentration in the surface layer which exceeds that in deep waters[9]. This suggests that its surface layer residence time is comparable with that of water. Thus it is likely that both these metals will exhibit fairly uniform distributions in open ocean surface waters despite their short oceanic residence times. The overall residence time of Fe corresponds to a settling rate of $4 \times 10^{-6}$ m s$^{-1}$ compared with $10^{-5}$ m s$^{-1}$ for particles containing $^{55}Fe$ (ref. 17). The equivalent Stokes particle size for inorganic detrital material is about 3 $\mu$m. Nevertheless, the primary host for downward transport of Fe in the open ocean is likely to be larger, lower density, biogenic particles, such as faecal pellets, with similar settling velocities.

Metals which remain predominantly in solution are removed from the water column considerably more slowly. Their distributions in the surface layer are probably controlled by mixing and metal incorporation into the biological components that are largely regenerated in the mixed layer. The deep water dissolved metal concentrations will be maintained by the degradation and dissolution of biogenic detritus and the balancing accumulation of metals on to exposed inorganic particle surfaces in the water column and in the sediments. The residence times of the predominantly dissolved metals, therefore, probably represent the time scales in which organic scavenging, biogenic particle settling and dissolution, and final association with inorganic particulate surfaces in the deep water are occurring.

Received 3 March; accepted 23 June 1977.


1 Coonley, L. S. T., Baker, E. B. & Holland, H. P. *Chem. Geol.* **7**, 51–62 (1971).
2 Boyle, E., Collier, R., Dengler, A. J., Edmond, J. M., Ng, A. C. & Stallard, R. F. *Geochim. cosmochim. Acta* **38**, 1719–1728 (1974).
3 Windom, H. L., Beck, K. O. & Smith, R. *Southeast Geol.* **12**, 169–181 (1971).
4 Holliday, L. M. & Liss, P. S. *Estuarine Coastal Mar. Sci.* **4**, 349–353 (1976).
5 Inman, C. L. & Nordstrom, C. E. *J. Geol.* **79**, 1–21 (1971).
6 Sundby, B. *Can. J. Earth Sci.* **11**, 1517–1533 (1974).
7 Holeman, J. N. *Water Resources Res.* **4**, 737–747 (1968).
8 Livingstone, D. A. *U.S. Geol. Survey Prof. Paper* 440-G (1963).
9 Bewers, J. M., Sundby, B. & Yeats, P. A. *Geochim. cosmochim. Acta* **40**, 687–696 (1976).
10 Sclater, F. R., Boyle, E. A. & Edmond, J. M. *Earth planet. Sci. Lett.* **31**, 119–128 (1976).
11 Boyle, E. A., Sclater, F. & Edmond, J. M. *Nature* **263**, 42–44 (1976).
12 Bender, M. L. & Gagner, C. *J. mar. Res.* **34**, 327–339 (1976).
13 Goldberg, E. D. & Arrenhius, G. *Geochim. cosmochim. Acta* **13**, 153–212 (1958).
14 Elderfield, H. *Mar. Chem.* **4**, 103–132 (1976).
15 Brewer, P. G. in *Chemical Oceanography* **1**, 2nd ed. (eds J. P. Riley, G. Skirrow,) 415–496 (1976).
16 Goldberg, E. D., Broecker, W. S., Gross, M. G. & Turekian, K. K. in *Radioactivity in the Marine Environment* 137–146 (National Academy of Sciences, 1971).
17 Labeyrie, L. D., Livingston, H. D. & Bowen, V. T. in *Transuranium Nuclides in the Environment* 121–135 (IAEA, Vienna, 1976).
18 Loring, D. H. *Can. J. Earth Sci.* **13**, 960–971 (1976).
19 Loring, D. H. *Can. J. Earth Sci.* **13**, 1706–1718 (1976).
20 El-Sabh, M. I. Report BI-R-75-9 (Bedford Institute of Oceanography, Dartmouth, Nova Scotia, Canada 1975).
21 Fairbridge, R. N. in *Encyclopedia of Geochemistry and Environmental Sciences* (Van Nostrand, New York, 1972).


# DNA arrangement in isometric phage heads


**W. C. Earnshaw**
Department of Biology, Massachusetts Institute of Technology, Cambridge, Massachusetts 02139

**S. C. Harrison**
Gibbs Laboratory, Harvard University, Cambridge, Massachusetts 02138


*DNA is wound tightly into phage heads in such a way that it tends to form layers concentric with the rigid protein shell. In P22 and wild-type lambda, DNA completely fills the internal volume, with a highly uniform local packing of adjacent segments; in lambda deletion mutants containing less than a full genome, the local packing distance increases correspondingly.*

DETERMINING the packing geometry of nucleic acid in virus particles presents a rather difficult experimental problem. In the heads of double-stranded DNA-containing bacteriophage, such as λ or P22, the nucleic acid is condensed 250-fold, and DNA strands are then so closely packed that conventional electron-microscopic techniques have yielded no interpretable images. Moreover, such phages are too large for application of the X-ray diffraction methods used to visualise single-stranded RNA in tobacco mosaic[1] and tomato bushy stunt viruses[2]. A large number of indirect approaches have been tried (see ref. 6), but virtually the only direct data bearing on the problem of DNA arrangement are those of Richards *et al.*[3], who managed to visualise gently disrupted bacteriophage particles in the electron microscope. They concluded that DNA

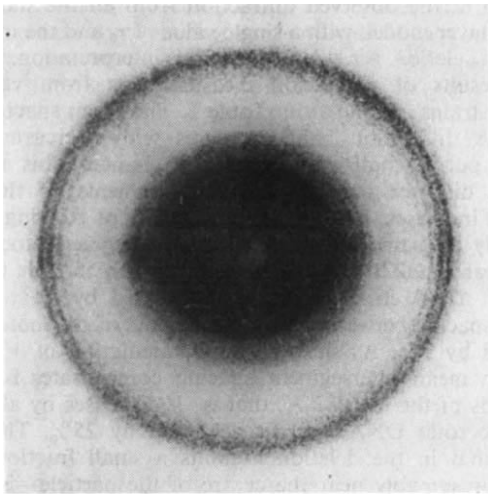

**Fig. 1** X-ray diffraction from phage P22. The outer set of rings corresponds to the 25 Å diffraction discussed in the text and shown as a scan in Fig. 2. The experimental conditions are described in ref. 4.

is coiled into the phage head—either coaxially like thread on a spool or with random direction like a ball of yarn. Recent small-angle X-ray scattering studies of intermediates in the P22 head-assembly pathway led us to recognise evidence for considerable long-range order in packaged DNA[4]. We describe here an extension of that work, leading to some conclusions about the organisation of DNA in bacteriophages with isometric heads—P22, λ and T7.

## Diffraction from phage

A photograph of X-ray diffraction from a solution of phage P22 is shown in Fig. 1. The series of rings at small angles can be interpreted in terms of the radial distribution of density in the particle[4]. They show that in first approximation, the P22 particle diffracts like a uniformly filled sphere. The strong outer band, corresponding to a spacing of about 25 Å in the structure, is due to DNA[4,5]. A densitometer trace of the intensity in this band is shown in Fig. 2. The diffraction is modulated by a series of ripples, having a periodicity approximately equal to the reciprocal of the head diameter. Experiments with other isometric phages (various strains of λ, T7) show this modulation to be not a mere superposition of other diffraction but rather a consequence of the geometry of DNA packing. Details of the interpretation of these observations are presented below. At wider angles, the diffraction from P22 and λ phage heads show the characteristic B-form DNA pattern, with maxima near 12, 8 and 3.4 Å (ref. 4).

## Organisation of phage DNA

The diffraction from phage DNA *in situ*, just described, reveals both local and long-range order in the phage head. The presence of local order, indicated by the strong 25-Å diffraction, ha sbeen recognised for some time[5,6]; the long-range order, indicated by the rippled modulation of this diffraction, was observed more recently by Earnshaw *et al.*[4], who first examined isometric phage with X-ray cameras of sufficient resolution.

Local order: adjacent segments of the DNA molecule are packed in a locally parallel array, with a side-to-side spacing that can be determined from the position of the 25-Å diffraction band[4]. From the width of this band, we can conclude that this spacing is quite uniform throughout the phage head with an 'apparent domain size' of −125 Å (refs 4, 5, 16). Assuming hexagonal packing, as in concentrated gels of DNA *in vitro*[7], the interhelix distance is equal to $1.16\delta$ where $\delta$ (~ 25 Å) is the spacing of the observed diffraction (Fig. 4 and Table 1, where the precise determination of $\delta$ from the pattern is described). We can also calculate the area of the local 'unit cell' (Fig. 4)—the cross-sectional area occupied by one DNA strand—this area, multiplied by the length of the P22 DNA molecules, gives the volume, $V$, taken up by the packed DNA. This calculated volume is in fact equal to the internal volume of the wild-type phage head, accurately determined from the structure of empty heads[4]. These calculations are summarised in the top line of Table 1.

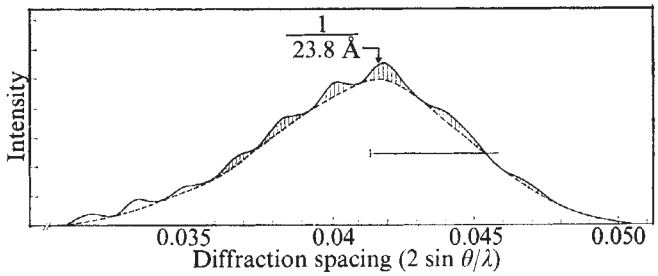


**Fig. 2** Densitometer trace in the 25-Å region of a film similar to the one shown in Fig. 1. The film was scanned as described in ref. 4. The shaded peaks are those used for fitting the model in Fig. 3. The horizontal bar indicates the half-width at half-height, 0.004 $Å^{-1}$. The data have been corrected by subtracting a smooth background due to diffuse scatter of the X-ray beam.

Long-range order: the ripples that modulate the intensity of the 25-Å diffraction have a wavelength of about 1/540 Å, that is, approximately the reciprocal of the internal diameter of the phage head. This indicates coherent diffraction from opposite sides of a particle: locally ordered DNA segments on one side must be diffracting with a fixed phase relative to locally ordered segments on the other. A linear DNA molecule

**Table 1** Measured and calculated dimensions for DNA packing in phage heads*

| Phage | | $d$ (Å) | $\delta$ (Å) | $A$ (Å²) | $l$ (Å) | $V$ (Å³) | $r$ (Å) | $r_0$ (Å) | $n$ | $f$ | ref. |
|---|---|---|---|---|---|---|---|---|---|---|---|
| P22 | | 24.2 | 23.8 | 638 | $14.0\times10^4$ | $8.9\times10^7$ | 278 | 278 | 4(+1) | 72 | 8 |
| λb221 | (78) | 26.2 | 25.8 | 772 | 12.6 | 9.75 | 285 | 294 | 5 | 90 | 9 |
| λb2 | (88) | 25.1 | 24.7 | 708 | 14.1 | 10.0 | 288 | 294 | 5 | 86 | 9 |
| λb515·b519 | (89) | 25.0 | 24.6 | 701 | 14.5 | 10.1 | 290 | — | — | — | 9 |
| λ+ | (100) | 24.0 | 23.6 | 647 | 16.1 | 10.4 | 292 | 294 | 5 | 80 | 9 |
| λ att² | (105) | 23.5 | 23.2 | 625 | 16.8 | 10.5 | 293 | 294 | 4 | 74 | 10 |

*$d$, mean Bragg spacing of DNA diffraction band measured from films; $\delta$, interlayer spacing, derived from $d$ by applying an approximate intensity-profile correction to account for the fact that the intensity maximum will be somewhat displaced from the reciprocal of the spacing between shells; $A$, area of local unit cell of DNA segment packing (cell assumed hexagonal, so that $A = 1.16\,\delta^2$); $l$, length of DNA; $V$, volume occupied by DNA in head ($V = A.l$); $r$, minimum radius to which DNA must extend, calculated from $V = (4/3)\,\pi r^3$; $r_0$, radius of DNA-protein boundary, calculated from best fit in Fig. 3 by adding 12 Å to the mean radius of the outermost DNA shell; $n$, number of DNA shells used for best fit to diffraction data (Fig. 3), in P22, a protein shell has also been included; $f$, fraction of total DNA in coherently scattering shells; ref. reference for DNA molecular weight.

The number in parenthesis after the name of the lambda phage strain indicates the percentage of wild-type DNA complement present. The genotype of λatt² was $i^{21}$.b515.b519.$int_2$.$xis_4$.att².bio⁺.uvrB⁺; all other λ strains were s7 (lysis-defective). Diffraction measurements were recorded from λ in 0.05 M NaCl, 0.1 M Tris-HCl (*p*H 7.4), 0.001 M $MgCl_2$ and from P22 in 0.01 M Tris-HCl (*p*H 7.5), 0.005 M $MgCl_2$.

is not likely to form a single crystal inside a spherical phage head (for example, the recent demonstration by Lerman *et al.* of the absence of chain-folding in ethanol-precipitated DNA[19]). Coherence across the phage particle must, therefore, be imposed by the regular, isometric protein shell within which the DNA is contained. Indeed, we would expect segments of the DNA molecule, locally parallel and tightly packed against the inner surface of the phage head, to fall into layers spaced regularly inward from the protein boundary. A spherically averaged picture of the particle will thus show distinct shells of density concentric with the protein shell itself. From the degree of local order implied by the intensity profile, we expect to see three or four such shells before packing irregularities destroy the uniformity of their diameter (Fig. 4). The same mode of packing continues at smaller radii, but packing faults become increasingly frequent.

The calculation presented in Fig. 3 shows that the ripples modulating DNA diffraction from P22 can indeed arise from a shell-like density fluctuation in the particle. The calculation assumes that $n$-concentric DNA layers, differing in radius by increments of $\delta$, are packed within the protein shell. This relatively tight shell[4] also contributes to the X-ray scattering since its inclusion in the calculation as a shell 24 Å from the outermost DNA layer improves the fit in Fig. 3. The radius of the outermost layer of DNA, 266 Å, has been chosen to achieve the best fit to the observed intensity profile. The radius of the boundary between DNA and protein, denoted $r_0$ in Fig. 4 and Table 1, can then be taken as this shell radius plus 12 Å (an estimate of the ionic radius of the DNA cylinder, see atomic coordinates in ref. 7). The parameters that best fit the intensity profile are $r_0 = 278$ Å and $n = 4$, where $\delta = 23.8$ Å has been determined directly from the mean spacing of the DNA diffraction band. This value of $r_0$ is, in fact, the same as the radius corresponding to $V$ (the calculated total DNA volume). Likewise, it is in accord with the inner radius of the protein shell, determined by small-angle X-ray scattering from empty heads[4].

The trace in Fig. 2 shows that the ripples modulating the 25-Å diffraction band account for about 15% of the total intensity. Since only one of the three (100) planes in the local hexagonal lattice (marked by arrows in the insert in Fig. 4) will contribute to this sampled diffraction, we expect the ripples to account for a maximum of one-third of the integrated intensity (actually somewhat less, since the outer layers account for only about 75% of the DNA molecule). Irregularities in the lattice and layer spacing will fill in the minima between ripples, so that the observed ratio of sampled to diffuse intensity is consistent with the picture drawn in Fig. 4. Note, that the envelope of the rippled intensity follows the diffuse diffraction: the local order is essentially the same in all directions, but the packing boundary imposed by a rigid head leads to a long-range radial regularity.

## Deletion mutants of phage λ

We have interpreted the diffraction from P22 phage DNA *in situ* in terms of locally parallel segments of DNA, packed tightly into the head in such a way that the polymer tends to form layers concentric with the outer protein shell. This model is summarised diagrammatically in Fig. 4. Further evidence for such a picture comes from measurements on a series of deletion mutants of bacteriophage λ. Unlike P22, which packages a constant headful of DNA, λ packages only the DNA between two distinct sites on the viral chromosome. As a result, genetic deletions result in production of phage heads containing less DNA. We have, in this way, obtained diffraction from structures with varying amounts of DNA packed into a head of constant size. The parameters of the model described above for P22 should be determined in a uniform way for the entire series of measurements on λ deletions: $r_0$ should be the same for all these structures, since it is in effect determined by the inner radius of the protein shell, and $d$ should be given by the mean spacing of the DNA diffraction band, as before. Our ability to fit the observed diffraction from all the stains by a simple $n$-layer model, with a single value of $r_0$ and the measured $\delta$ for each deletion, is a strong test of this interpretation.

The results of diffraction measurements from various λ deletion strains are shown in Table 1. The mean spacing, $d$, of the DNA diffraction band increases with decreasing DNA content, but its half-width does not change. This indicates that the distance between adjacent segments of the DNA molecule increases, but that the uniformity of packing remains essentially the same. In other words, the degree of local order is as great in b221 as in wild-type λ, even though the total length of DNA in the head has decreased by 22% and the average spacing between adjacent segments of the molecule has increased by 9%. As shown by the calculation of $V$, the increase in mean intersegment spacing compensates for about two-thirds of the lost DNA, that is, $V$ decreases by about 7% when the total DNA content decreases by 25%. This result implies that in the deletion mutants a small fraction of the DNA—presumably near the centre of the particle—is packed more loosely than the rest.

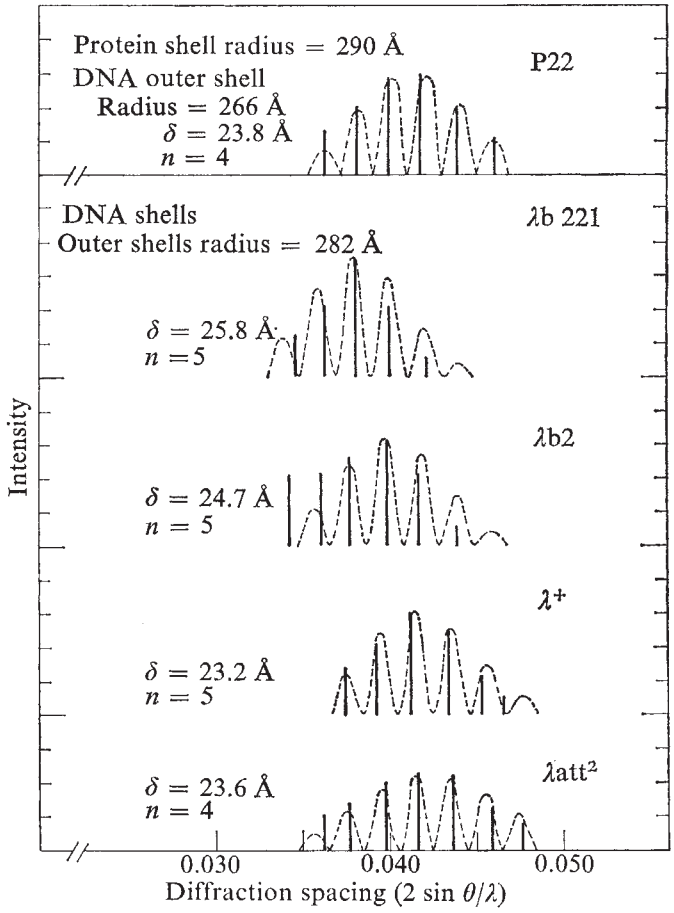


**Fig. 3** Correspondence of model calculations to observed diffraction for phage 22 and various λ mutants. Spikes represent position and scaled height of intensity maxima (shaded ripples in Fig. 2); – – – – shows scattered intensity calculated for a series of concentric shells[16], with each shell weighted according to the amount of scattering material it contains. The calculated intensity equals $F^2$, where

$$F = \sum_{i=1}^{m} 4\pi r_i^2 \left(\frac{\sin 2\pi r_i s}{2\pi r_i s}\right)$$

and $r_i$ is the radius of the $i$th shell ($m$ in all) and $s = 2\sin\theta/\lambda$, the diffraction spacing. There are $n$ shells of DNA spaced $\delta$Å apart, and in the case of P22 a shell for protein has also been included. For λ mutants, where head size is constant, we have assumed a fixed radius of 282 Å for the outer DNA shell: to obtain $r_0$, the DNA-protein boundary, 12 Å must be added to this figure.

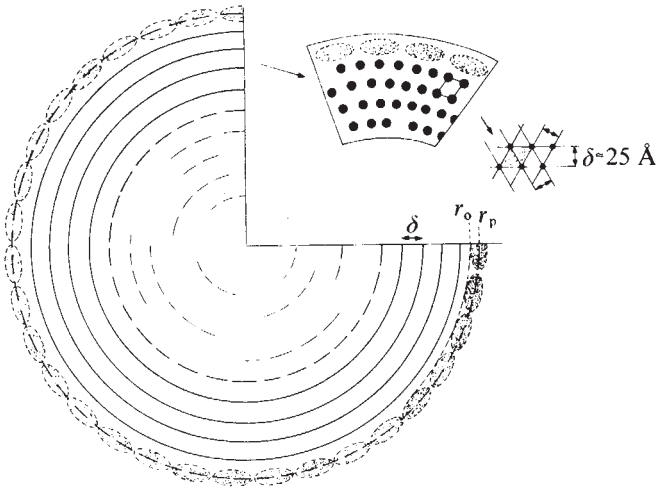


**Fig. 4** Diagrammatic representation of the model used to obtain curves in Fig. 3. The protein (radius = $r_p$) is shown stippled; the radius of the DNA-protein boundary is $r_0$; the inter-shell spacing is δ. Adjacent segments of the DNA helix are parallel, with the local unit cell assumed to be hexagonal[7,19]. If this is the case, packing faults must be introduced in inner shells, as shown. For this reason, the innermost DNA is shown as partially organised shells, though it could be packed in some other manner. For phage P22 the model includes a shell at radius $r_p$ and four inner shells with spacing δ. For the λ mutants the model includes five shells with spacing δ, the outer shell at a radius of 282 Å.

All strains studied show the same rippled modulation of the DNA diffraction described above for P22. The spacing between these ripples remains essentially constant with varying DNA content, but the positions of the maxima and minima shift, as indicated in Fig. 3. The results in Table 1 and Fig. 3 show that we can fit all observations by models with four or five coherently scattering layers, without changing $r_0$. That is, we can imagine an outer layer of DNA segments, packed tightly against a protein shell of fixed size, and successive layers of segments packed against the first with a spacing that increases with decreasing DNA content. Moreover, the best value of $r_0$ for all strains agrees well with the inner radius of urea-treated A⁻petit λ, an *in vitro* analogue of empty heads (Earnshaw and Hendrix, in preparation). In contrast with P22, the protein shell itself does not appear to contribute to the 25 Å diffraction, and it has not been included in the model calculation.

The fraction of the DNA molecule that would be contained in these coherently-diffracting layers varies from about 90% for b221 to about 75% for att[2] (Table 1). In all cases, then, a large fraction of the molecule is packed in this way. There are probably several further layers, but at this distance from the constraining walls of the phage head, the segments would be sufficiently out of register that they would not contribute to ripples in the 25-Å diffraction.

The results from λ strains in Table 1 refer to phage in 0.05 M NaCl, 0.01 M Tris (*p*H 7.4), 0.001 M $MgCl_2$. Substitution of 0.01 M polyamine (spermidine or putrescine) for $Mg^{2+}$ has no effect on the measured spacings. Moreover, diffraction from intracellular λb2.s7 accumulating in unlysed su⁻ cells shows the 25 Å band quite clearly. We conclude, as we did earlier for P22[4], that the arrangement of DNA in a phage head does not change when lysis alters its ionic environment. Polyamine may, however, be important for the initial packaging event[11].

## Three dimensions

What more detailed pictures of DNA packing are consistent with the picture presented above? The electron micrographs of gently-disrupted phage heads obtained by Richards *et al.*[3] show unexpanded DNA bundles, flattened into the grid: DNA strands near the periphery of these bundles always have a circumferential orientation. These micrographs suggest that DNA is not folded with sharp kinks inside the phage head, but rather, that it is wound with relatively uniform curvature. Richards *et al.*[3] proposed two limiting descriptions of DNA in phage heads based on these images: a 'ball of string' and a 'concentric spool'. In the first (Fig. 5*a*), DNA is wound roughly along a great circle path at any radius, with no particular relation of the tilt of the planes of successive great circular windings. In the second (Fig. 5*b*), the molecular windings are concentric with a single axis. Our observations seem to be inconsistent with the ball-of-string picture. The crossing of successive turns in a ball of string does not lead to parallel adjacent strands or to radially concentric layers. Such crossing also leaves gaps too large to be compatible with the tight packing of DNA in the head. Coaxial winding does not present these difficulties: segments are locally parallel and closely packed. Our data do not specify the relative orientation of these windings and the axis of the phage tail.

Certain folded structures might also be consistent with an overall organisation into shells of DNA segments layered inward from the protein, provided that the folds were appropriately positioned (Fig. 5*c*). Folds could plausibly result only from interaction of DNA with specific sites on the inner surface of protein subunits. The continuous variation of DNA spacings observed in λ deletions is difficult to reconcile with a fixed set of folding positions. Moreover, the local symmetry of the protein surface lattice implies that only radially-directed DNA can have an equivalent orientation with respect to each folding site: the uniformity of packing we have observed rules out a radial direction. Finally, we would not expect folded structures, when flattened on to an electron microscope grid, to show the images of coiled, circumferentially-directed strands seen by Richards *et al.*[3]. For these reasons, we prefer the coiled structure shown in Fig. 5*b*.

In any structure with more or less uniformly bent DNA, the stiffness of the polymer will prevent windings of very small radius, leaving a roughly cylindrical cavity in the centre of the head (Fig. 5*b*). Changes in packing of DNA in this region—estimated below to be less than 10% of the total volume of the head—might account for the slight decrease in $V$ with decreasing DNA content. This could also account for the region of low density seen in the centre of λ and λ*dg* in ultra-thin sections in the electron microscope[18]. A reasonable value for $r_{min}$, the radius of the cylindrical cavity, is the radius of a circle of DNA for which the bending enthalpy equals ~ 7 kcal $mol^{-1}$—an estimate for the enthalpy of a single 180°

**Fig. 5** Schematic representation of various models discussed in the text. *a* Ball-of-string. *b* Coaxial spool. *c* Chain-folded structure (with 180° folds at each end).

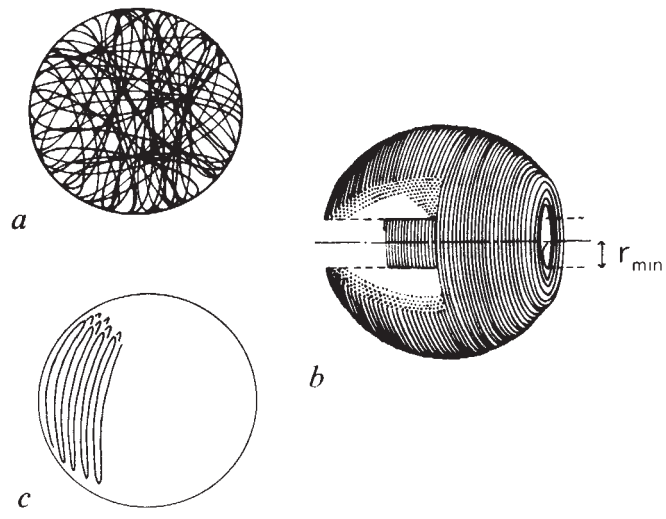

fold[12]. The bending enthalpy of DNA was determined by Gray and Hearst[13]: their figure of $\Delta H_{bend} = 75$ kcal Å mol$^{-1}$ rad$^{-2}$ is applicable, strictly speaking, only to radii of curvature comparable with the solution persistence length (~ 500 Å), but its use with rather smaller radii seems adequate, since even for $r = 50$ Å the bend is only about 4° per base pair. With this value for $\Delta H_{bend}$, we get $r_{min} \sim 60$ Å. Also, using this estimate of $r_{min}$, integration over the total occupied volume yields $\Delta H_{tot} = 4\pi(\Delta H_{bend}/A))(r\ln(2r_0/r_{min}-\frac{1}{2})-r_0+r_{min}/2) \sim 500$ kcal (where $A$ and $r_0$ taken here as 647 Å$^2$ and 294 Å, appropriate for λ, are defined in Table 1 and Fig. 4). To fold DNA into a λ head would require more than $l/2r_0$ folds ($l$ is the DNA length; $2r_0$, the head internal diameter)—more than 2,000 kcal. The cylindrical cavity defined by $r_{min}$ contains about 9% of the total volume. The column $V$ in Table 1 shows that in λb221, only about 91% of the total volume inside $r_0 = 294$ Å is required for DNA packed with spacing $\delta = 25.8$ Å. In this extreme deletion, then, the central regions might actually be nearly free of DNA. In other forms, a larger fraction of the total volume is required (all of it in wild type and att$^2$). In these structures, most of the DNA can be coiled into cylindrically concentric shells, but up to 10% might be folded back and forth lengthwise in the central region (a possibility suggested to J. Schellman), perhaps passing from there to the phage tail (see cross-linking experiments with λ and other phages—refs 14 and 15).

We thank Jonathan King for continuing interest and valuable advice and Gerard Bricogne, John Schellman, and R. Kornberg for helpful discussions. Phage samples were gifts of Roger Hendrix (λ b221), Mark Ptashne and Andrea Jeffrey (λb2), William McClure (λ$^+$, T7), Susan Gottesman (λatt$^2$), and Phillip Youderian (λ n515 b519). We thank Jonathan King and David Botstein for useful criticism of the manuscript. We acknowledge grant support from the National Cancer Institute (to S.C.H.) and from the National Institute of General Medical Sciences (to J. K.), an NSF Predoctoral Fellowship (to W. C. E.), and a PHS Research Career Development Award (to S.C.H.).

Received 10 February; accepted 19 May 1977.

1 Holmes, K. C., Stubbs, G. J., Mandelkow, E. & Gallwitz, U. *Nature* **254**, 192–196 (1975).
2 Winkler, F. K., Schutt, E. E., Bricogne, G. & Harrison, S. C. *Nature* **265**, 509–513 (1977).
3 Richards, K., Williams, R. & Calendar, R. *J. molec. Biol.* **78**, 255–259 (1973).
4 Earnshaw, W. C., Casjens, S. & Harrison, S. C. *J. molec. Biol.* **104**, 387–410 (1976).
5 North, A. C. T. & Rich, A. *Nature* **191**, 1242–1245 (1961).
6 Tikchonenko, T. I. in *Comprehensive Virology* (eds Fraenkel-Conrat, H. & Wagner, R. R.) 5 (Plenum, New York, 1975).
7 Luzzati, V. & Nicolaieff, A. *J. molec. Biol.* **1**, 127–133 (1959).
8 Rhoades, M., MacHattie, L. A. & Thomas, C. A. *J. molec. Biol.* **37**, 21–40 (1968).
9 Davidson, N. and Szybalski, W. in *The Bacteriophage Lambda* (ed. A. D. Hershey), (Cold Spring Harbor, New York, 1971).
10 Fiandt, M., Gottesman, M. E., Schulman, M. J., Szybalski, E. H., Szybalski, W. & Weisberg, R. A. *Virology* **72**, 6–12 (1976).
11 Gosule, L. C. & Schellman, J. A. *Nature* **259**, 333–335 (1976).
12 Bloomfield, V., Crothers, D. M. & Tinoco, I., Jr. *Physical Chemistry of Nucleic Acids* (Harper & Row, New York, 1974).
13 Gray, H. B., Jr. & Hearst, J. E. *J. molec. Biol.* **35**, 111–129 (1968).
14 Thomas, J. O. *J. Molec. Biol.* **87**, 1–9 (1974).
15 Chattoraj, D. K. & Inman, R. B. *J. molec. Biol.* **87**, 11–22 (1974).
16 Guinier, A. *X-Ray Diffraction in Crystals, Imperfect Crystals and Amorphous Bodies* (W. H. Freeman and Co., San Francisco, 1963).
17 Arnott, S. *Prog. biophys. molec. Biol.* **21**, 265–319 (1970).
18 Cummings, D. J., Chapman, V. A. & DeLong, S. S. *J. molec. Biol.* **14**, 418–422 (1965).
19 Lerman, L. S., Wilkerson, L. S., Venable, J. H., Jr & Robinson, B. H. *J. molec. Biol.* **108**, 271–293 (1976).

# Initiation of chick cell division by trypsin action at the cell surface

**Darrell H. Carney & Dennis D. Cunningham**

Department of Medical Microbiology, College of Medicine, University of California, Irvine, Irvine, California 92717

*Trypsin immobilised on polystyrene beads causes initiation of cell division which cannot be accounted for by trypsin released into the medium or into the cells. Also, initiation by soluble trypsin is inhibited by immobilised soybean trypsin inhibitor. These results demonstrate that trypsin can initiate proliferation at the cell surface.*

THE site of action of peptide hormones and certain growth factors is often presumed to be at the cell surface. Indeed, binding studies and isolation of binding proteins by affinity chromatography have demonstrated that specific receptors for these molecules exist in the plasma membrane. Such receptors might be involved primarily in transport or other functions, however. For example, it has been shown that there are cell surface receptors for steroid hormones even though their site of action is clearly inside the cell[1]. There are reports that certain peptide hormones and growth promoters can act without entering cells [2–6], but most of this evidence has been obtained with Sepharose-immobilised preparations. The validity of these studies has been challenged[7–10] primarily because of the amount of soluble material released[7,8] and because such material may be 'superactive'[10]. Therefore, it is still questionable whether peptide factors can exert their biological effects without entering cells.

Trypsin and certain other proteases initiate proliferation of cultured quiescent chick embryo fibroblasts (CEF) (refs 11-18). This system has two important advantages for studying the mechanisms involved in initiation of cell proliferation. First, the initiation occurs in serum-free medium without additional growth factors[13], and second, it is caused by purified agents with well characterised proteolytic activities. In spite of these advantages, little progress has been made towards elucidating the actual mechanisms involved. It has been reported that 5-min treatments with soluble proteases or proteases linked to Sepharose beads doubles the number of mouse 3T3 cells[19–21]. This would suggest that trypsin acts at the cell surface. But other investigators have not achieved significant initiation of 3T3 cell division with trypsin using various experimental conditions including exposures of up to several days[17, 22, 23]. Even in chick cells, whose division is readily stimulated by trypsin, the protease must be present for at least 2 h to cause a significant increase in cell number, and the fraction of cells which respond increases with length of exposure up to 24 h (refs 17, 18). Such lengthy exposure times suggest a more complex mechanism of initiation than the simple binding or cleavage of specific receptors. Indeed, it has not been possible to correlate cleavage of specific surface membrane proteins with initiation of proliferation by proteases[14–16, 24]. Moreover, both thrombin (ref. 25 and B. M. Martin and J. P. Quigley, personal communication) and trypsin[26] accumulate inside cultured cells after exposures sufficient to initiate cell division. These considerations prompted us to develop techniques to rigorously determine if trypsin could initiate proliferation of chick fibroblasts without entering the cells.

We report here that trypsin covalently attached to poly-